SCIENTIFIC REPORTS

OPEN

Evidence for in-gap surface states on the single phase $SmB_6(001)$ surface

Received: 13 June 2017
Accepted: 14 September 2017
Published online: 09 October 2017

Toshio Miyamachi[1], Shigemasa Suga[2,3], Martin Ellguth[4], Christian Tusche[3,5], Claus M. Schneider[3,5], Fumitoshi Iga[6] & Fumio Komori[1]

Structural and electronic properties of the $SmB_6(001)$ single-crystal surface prepared by Ar^+ ion sputtering and controlled annealing are investigated by scanning tunneling microscopy. In contrast to the cases of cleaved surfaces, we observe a single phase surface with a non-reconstructed $p(1 \times 1)$ lattice on the entire surface at an optimized annealing temperature. The surface is identified as Sm-terminated on the basis of spectroscopic measurements. On a structurally uniform surface, the emergence of the in-gap state, a robust surface state against structural variation, is further confirmed inside a Kondo hybridization gap at 4.4 K by temperature and atomically-resolved spatial dependences of the differential conductance spectrum near the Fermi energy.

The Kondo insulator samarium hexaboride (SmB_6) has attracted great attention over decades due to its strong electron correlation. It exhibits a metal-insulator transition with decreasing temperature as a consequence of a gap opening triggered by the hybridization of localized 4f states with itinerant 5d states[1]. A particular interest is directed to the plateau in the electrical resistivity in the low temperature regime (< 5 K)[2]. An in-gap state inside the Kondo hybridization gap was proposed as a possible origin of this resistance plateau[3]. Theoretical predictions that SmB_6 is a promising candidate for a topological Kondo insulator with a topologically protected surface state[4,5] revive the intense interest in experimental studies to identify the origin of the in-gap state[6,7]. However, spatially-resolved surface characterizations by scanning tunneling microscopy (STM) have revealed that several types of surface structures randomly coexist on the cleaved $SmB_6(001)$ surfaces[8–12]. This hampers the investigation of its intrinsic surface electronic properties by spatially-integrated methods. Furthermore, the cleavage of SmB_6 results in non-reproducible relative weight of the surface structures, prohibiting reliable discussion on electronic as well as atomic structures of the prepared surface. Thus, the establishment of a new reproducible preparation method of the single phase SmB_6 surface at least over sub-μm^2 is mandatory not only from the viewpoint of the fundamental material science but also from the application point of view. As an alternative to the crystal cleavage, a cyclic Ar^+ ion sputtering and subsequent annealing is recently proposed to reproducibly prepare a single-phase $SmB_6(001)$ surface by spatially-integrated observations with low energy electron diffraction (LEED)[13]. Nevertheless, the atomic structure of such a surface still remains to be confirmed for detailed discussion of its in-gap surface state because a non-reconstructed $p(1 \times 1)$ LEED pattern could appear for disordered $SmB_6(001)$ surface[14]. Furthermore, previous LEED studies have reported the existence of superstructures even on the surface prepared by this method[15,16], which implies the difficulty of controlling appropriate preparation conditions.

In this study, we report real-space STM characterizations of a single-phase $SmB_6(001)$ surface prepared by a cyclic Ar^+ ion sputtering and optimally controlled annealing on the atomic scale with a reliable evaluation of its in-gap state. We find that the surface quality is gradually improved when increasing annealing temperature up to 1030 °C. Atomically-resolved STM observations combined with spectroscopic measurements have revealed that at an optimized annealing temperature the entire surface is composed of a non-reconstructed $p(1 \times 1)$ lattice with Sm-termination. Furthermore, temperature and atomically-resolved spatial dependences of the differential

[1]The Institute for Solid State Physics, The University of Tokyo, Kashiwa, Chiba, 277-8581, Japan. [2]Institute of Scientific and Industrial Research, Osaka University, Ibaraki, Osaka, 567-0047, Japan. [3]Peter Grünberg Institut (PGI-6), Forschungszentrum Jülich, 52425, Jülich, Germany. [4]Institut für Physik, Johannes-Gutenberg-University, Mainz, 55128, Mainz, Germany. [5]Fakultät für Physik, Universität Duisburg-Essen, 47057, Duisburg, Germany. [6]College of Science, Ibaraki University, Mito, Ibaraki, 310-0056, Japan. Correspondence and requests for materials should be addressed to T.M. (email: toshio.miyamachi@issp.u-tokyo.ac.jp)

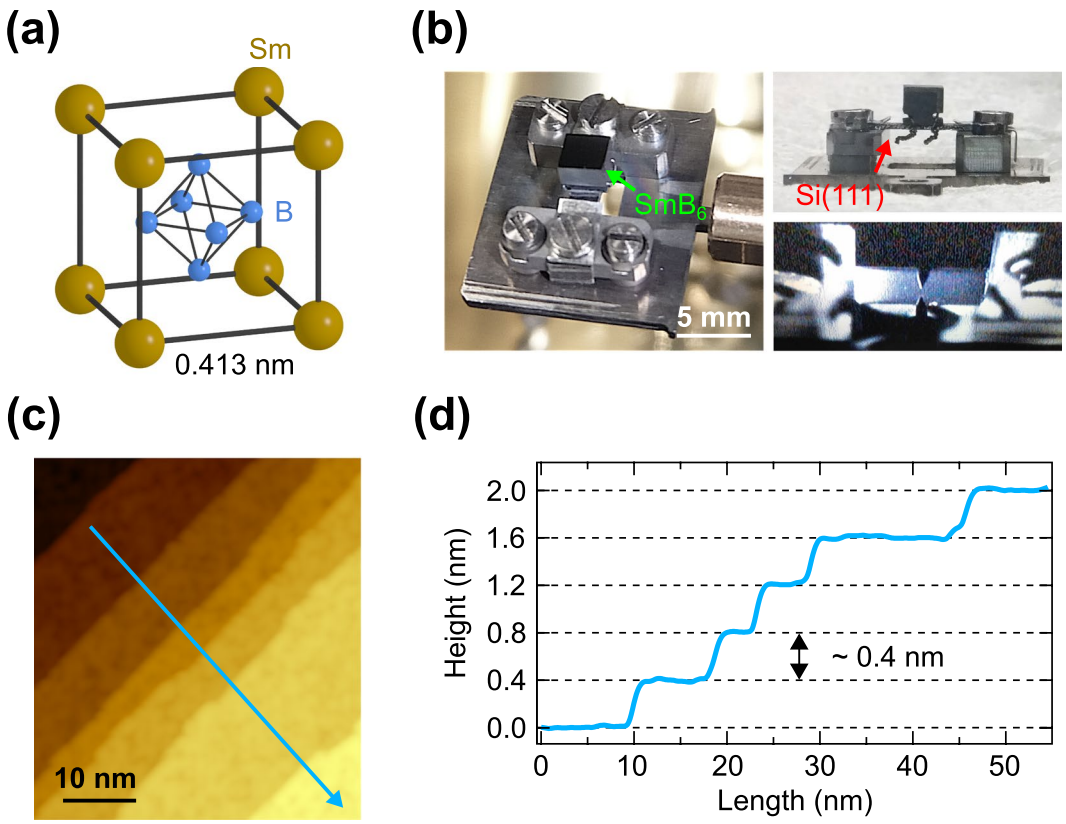

Figure 1. (**a**) Schematic crystal structure of SmB_6. (**b**) Photographs of the $SmB_6(001)$ single crystal and its mounting. (**c**) STM image of the $SmB_6(001)$ surface annealed at 1030 °C. (**d**) STM height profile of atomic steps along the blue line in (**c**). The interval between the grid lines in height is nearly equal to the lattice constant of SmB_6.

conductance spectrum near the Fermi energy identify the in-gap state with a characteristic peak-dip feature emerging inside the Kondo hybridization gap at 4.4 K as a robust surface state against structural variation.

Results

The crystal structure of SmB_6 is schematically displayed in Fig. 1(a). In the CsCl-type structure, one Sm atom and one B_6 octahedron occupy the cubic lattice with the lattice constant of 0.413 nm. Figure 1(b) displays photographs of the $SmB_6(001)$ single crystal in this study, which is fixed to a Si(111) substrate and mounted to the STM sample holder. Note that the single crystal is annealed via direct current heating of the Si(111) substrate. The flatness of the surface can be recognized from a mirror image of the STM tip approaching from the bottom. Atomic steps are indeed visible in an STM image of the $SmB_6(001)$ surface prepared by Ar^+ ion sputtering and subsequent annealing at 1030 °C as shown in Fig. 1(c). The corresponding STM height profile shown in Fig. 1(d) clearly gives the step height of ~ 0.4 nm nearly identical to the lattice constant of the $SmB_6(001)$ plane.

We first investigate the annealing temperature dependence of the $SmB_6(001)$ surface. A series of the $SmB_6(001)$ surfaces annealed at 900, 980 and 1030 °C are displayed in Fig. 2(a). While terraces are separated by monatomic steps for all the annealing temperatures, we find clear differences in the density of defects on the surface. At 900 °C, the surface is composed of small islands with a high density of defects. At higher temperature annealing, the coalescence of the islands is promoted, resulting in the reduction of the defect density. The surface quality is considerably improved after 1030 °C annealing. Since Ar^+ ion sputtering increases the concentration of Sm atoms near the surface[13], the annealing process reduces the defect density and flattens the surface with a Sm-termination. The fraction of the topmost layer, f_{top}, as a function of the annealing temperature is plotted in Fig. 2(b). An extrapolation of a monotonous increase of f_{top} with the annealing temperature gives the maximum f_{top} at 1080 °C, in line with the evaluation of the quality of the Sm-terminated surface by a Sm/B Auger peak ratio[13].

To get further insights into the $SmB_6(001)$ surface, we focus on the defect depth. Figure 2(c) displays typical STM line profiles on the surface annealed at 900 and 1030 °C. After annealing at 900 °C, a wide range of the depth distribution of more than one lattice constant (~ 0.4 nm) is observed, strongly implying the presence of several types of surface terminations. After annealing at 1030 °C, however, the defects show only one level of ~ 80 pm in depth, corresponding well to the height difference between the Sm plane and the underlying topmost B atom in the B_6 octahedron on the Sm-terminated surface as reported for cleaved samples[10] [see also Fig. 1(a)]. Taking the lower vaporization energy of Sm relative to B into consideration[17], annealing at 1030 °C or up to 1080 °C improves the surface quality by filling the defect sites with the Sm atoms.

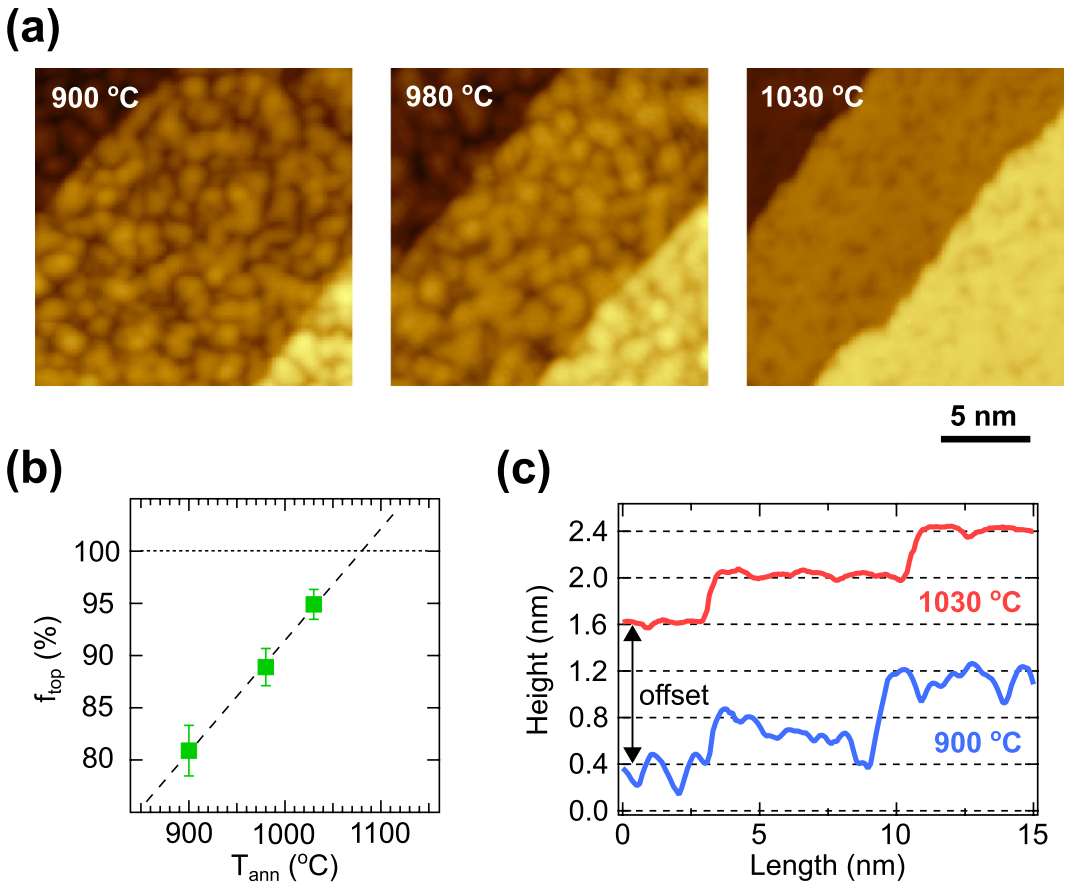

Figure 2. (**a**) STM images of the $SmB_6(001)$ surface annealed at 900, 980 and 1030 °C. (**b**) f_{top} values as a function of the annealing temperature with the least squares fit. (**c**) Typical STM height profiles of the $SmB_6(001)$ surface annealed at 900 and 1030 °C. The interval between the grid lines in height is nearly equal to the lattice constant of SmB_6.

We have further confirmed that the observed annealing temperature dependence is consistently reflected in a macroscopic scale. Figure 3(a) and (b) display large scale STM images of the $SmB_6(001)$ surface annealed at 900 and 1030 °C. Both surfaces exhibit similar vicinal structures with a high density of atomic steps, which arise from the slight miscut angle of the crystal from the [001] direction. However, the LEED pattern of the surface changed drastically with increasing annealing temperature as compared between Fig. 3(c) and (d). The complex LEED pattern of the sample annealed at 900 °C strongly indicates the coexistence of several types of reconstructed surfaces, e.g., $c(2 \times 2)$, (1×2) or (2×1) reconstructions, in line with the interpretation of the STM observations in Fig. 2. In contrast, the LEED pattern after 1030 °C annealing shows a $p(1 \times 1)$ structure with no additional superstructure spots in the measured energy range between 15 and 120 eV. The faint streaks appearing in the LEED pattern at this annealing temperature reflect the alignment of the steps in one direction [see also Fig. 3(a) and (b)]. Still no obvious difference in the terrace width is observed between the surfaces annealed at 900 and 1030 °C. Thus, the role of high-density steps acting as strain relievers to stabilize the surface lattice[18] is minor, and the annealing at an optimized temperature is essential for the formation of the $p(1 \times 1)$ lattice. Note that each LEED pattern is measured immediately after the STM observations, and thus a degradation of the surface can be excluded as a possible origin of the change in the LEED pattern[14].

The annealing temperature dependence investigated by STM and LEED reveals that the surface quality improves gradually when raising annealing temperature, and the single phase $SmB_6(001)$ surface with a non-reconstructed $p(1 \times 1)$ lattice emerges on the entire surface at around 1030 °C. We have then performed atomically-resolved STM observations of the $SmB_6(001)$ surface to check the surface termination. Atomic-scale ordered structures of the non-reconstructed $SmB_6(001)$ surface with Sm- and B- terminations have been reported by STM previously on the cleaved surfaces[8–12]. The B-terminated surface derived from B apex atoms in the B_6 octahedra exhibits a periodicity corresponding to the lattice constant of SmB_6. On the Sm-terminated surface, however, a lattice with alternating rows of Sm and B atoms with different heights would appear due to the existence of Sm and B sublattices, leading to a periodicity with $1/\sqrt{2}$ of the SmB_6 lattice constant[9].

Figure 4(a) displays an atomically-resolved STM image of the $SmB_6(001)$ surface annealed at 1030 °C. We still observe a non-negligible amount of defects, which induces the local disorder on the surface. A relatively ordered region zoomed from the dashed rectangle region in Fig. 4(a) is displayed in Fig. 4(b), forming the non-reconstructed $p(1 \times 1)$ lattice as confirmed by LEED. However, the STM height profile shown in Fig. 4(c) reveals that the lateral periodicity of the $p(1 \times 1)$ lattice distributes between 300 and 500 pm. Furthermore, its

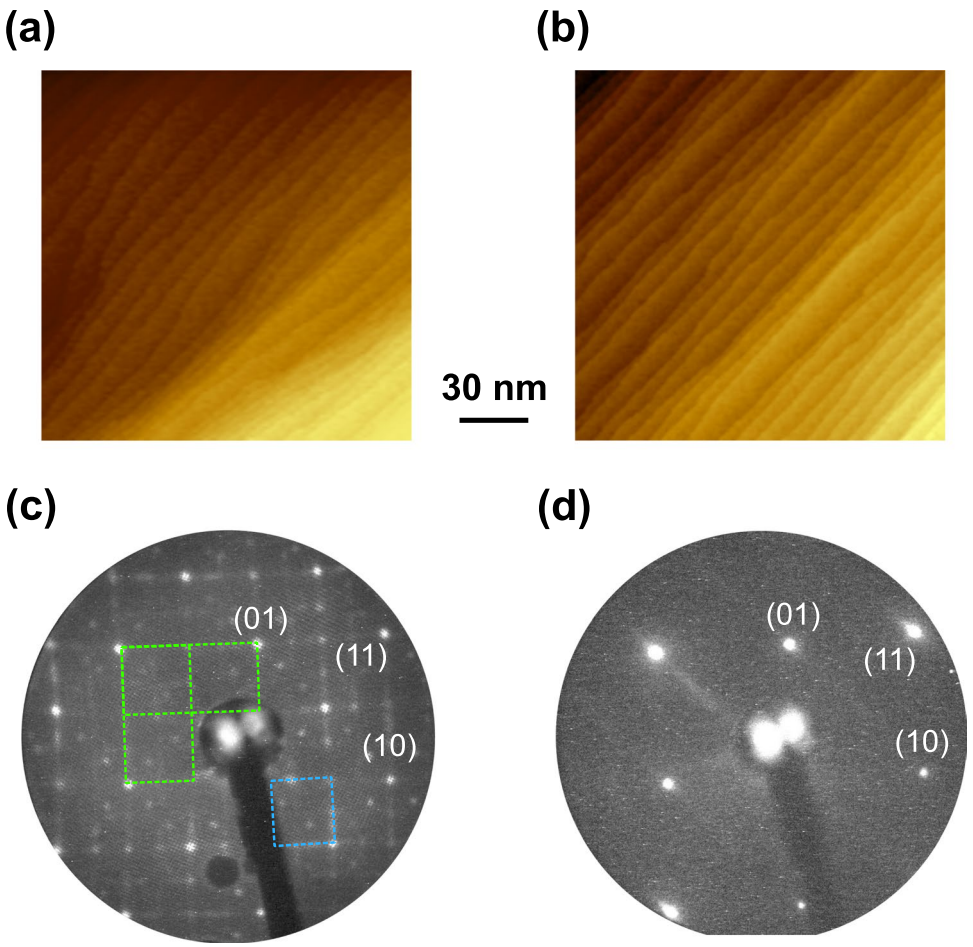

Figure 3. Large scale STM images of the SmB_6(001) surface annealed at (**a**) 900 and (**b**) 1030 °C. (**c**) LEED pattern of the sample annealed at 900 °C. Superstructure spots of $c(2 \times 2)$ and (1×2) or (2×1) are indicated by blue and green rectangles. (**d**) LEED pattern of the sample annealed at 1030 °C. LEED patterns are taken at the electron energy of 38 eV.

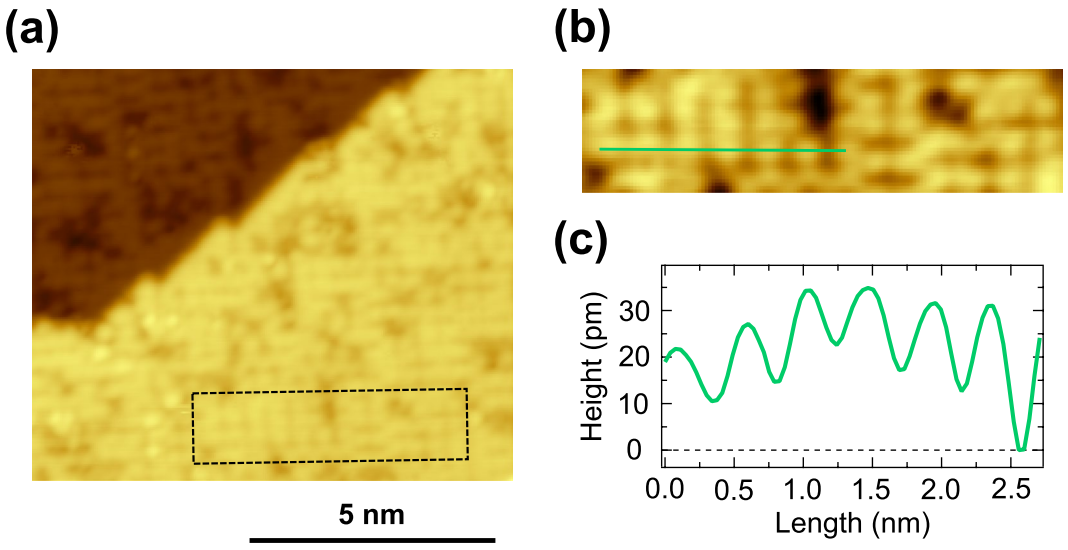

Figure 4. (**a**) Atomically-resolved STM image of the SmB_6(001) surface annealed at 1030 °C. (**b**) Zoomed STM image from (**a**). The image size corresponds to the rectangle in (**a**). (**c**) STM height profile along the green line in (**b**).

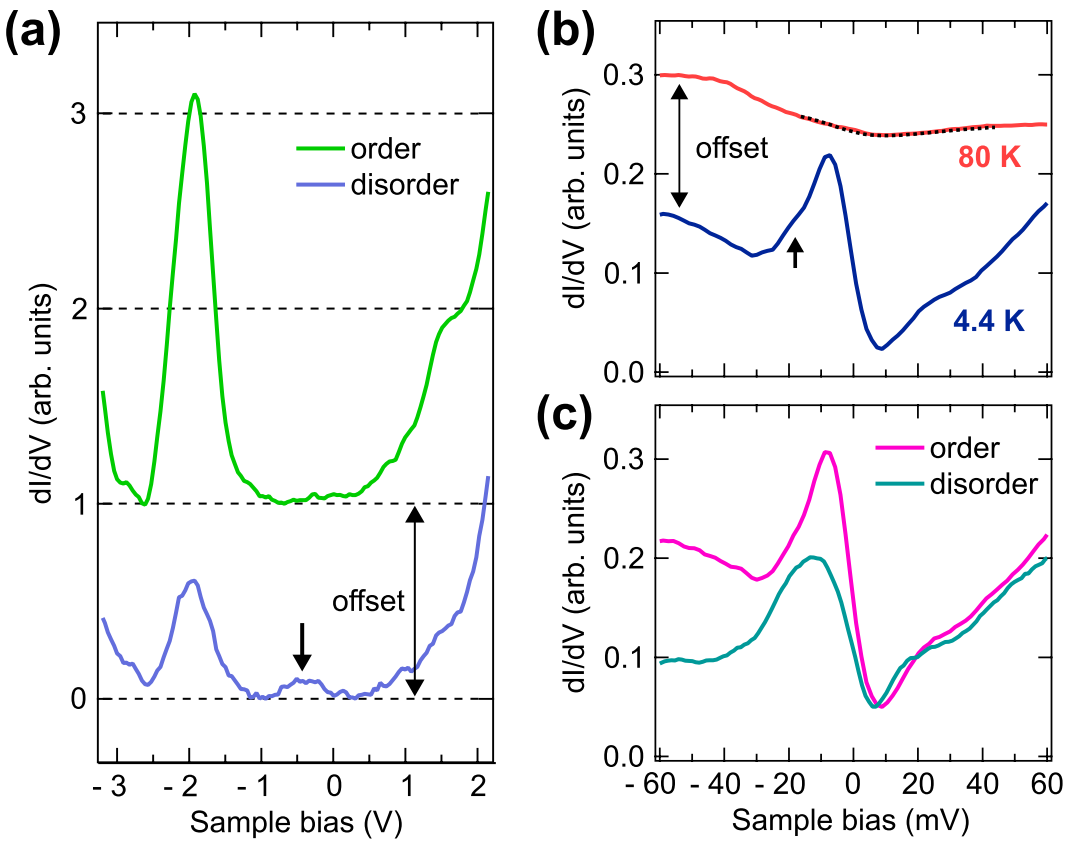

Figure 5. (**a**) dI/dV spectra over a wide range of sample bias from −3.2 V to 2.2 V recorded on ordered (Sm-terminated), and disordered regions at T = 80 K. The arrow indicates the broad feature. (**b**) Temperature dependence of the spatially averaged dI/dV spectra near the Fermi energy. The dotted line on the dI/dV spectrum at T = 80 K is a Fano fit (see text) with a q-factor of 0.56, Γ of 21.6 ± 0.6 meV and E_0 of ~ 8 meV. The arrow indicates the fine shoulder structure possibly derived from localized bulk f-states. (**c**) Spatial dependence of the dI/dV spectra near the Fermi energy recorded on the ordered region, and the disordered region near defects.

height changes non-systematically. Thus, the surface disorder caused by a certain amount of defects makes it difficult to determine the surface termination only by atomically-resolved STM observations. Note that the maximum annealing temperature in this study is restricted up to ~1030 °C since the temperature of the underlying Si(111) substrate nearly reaches its melting point of ~1200 °C[19–21], although further increasing annealing temperature may decrease the defect density and improve the surface quality.

Spectroscopic measurements can also play a crucial role to determine the surface termination. We especially focus on the energy level of the surface state derived from the B 2p dangling bonds. An angle-resolved photoemission (ARPES) study supported by density functional theory revealed that the energy level of the B 2p surface state depends strongly on the surface termination, i.e, it is located near the Fermi energy for the B-terminated surface, while it shifts about 2 eV below the Fermi energy for the Sm-terminated surface[13,22]. Figure 5(a) displays the dI/dV spectra of the SmB_6(001) surface annealed at 1030 °C for both on ordered regions and on disordered regions near defects. Being independent of the surface quality, a common peak structure located at −2.0 V is observed. Its energy level corresponds nicely to that of the surface state derived from the B 2p dangling bonds on a Sm-terminated surface. Thus, combining with the results of atomically-resolved STM observations shown in Fig. 4, we conclude the Sm-terminated single phase with non-reconstructed $p(1 \times 1)$ lattice is formed on the SmB_6(001) surface prepared by Ar^+ ion sputtering and annealing at an optimized temperature.

The structural information on the SmB_6(001) surface could be further extracted from the spatial dependence of the B 2p peak intensity. We find that the B 2p peak intensity is weak on disordered regions near defects. In addition, a feature located at around −0.5 V is occasionally observed in the dI/dV spectrum as indicated by an arrow in Fig. 5(a). On the other hand, the feature (−0.5 V) disappears in the dI/dV spectrum with the strong B 2p peak intensity on ordered regions. A similar tendency is reported on a cleaved SmB_6(001) surface, and is interpreted in terms of the existence of disordered regions with random Sm- and B- terminations[22]. Thus, in accord with atomically-resolved STM observations shown in Fig. 4, the observed spatial dependence of the B 2p peak intensity in the dI/dV spectra in Fig. 5(a) is attributed to the degree of surface disorder caused by defects.

Finally, we discuss the electronic properties of the SmB_6(001) surface near the Fermi energy. Figure 5(b) displays the temperature dependence of the dI/dV spectrum near the Fermi energy. At 80 K, the dI/dV spectrum exhibits a typical asymmetric lineshape interpreted as the Kondo hybridization gap[6,7,9,12]. The asymmetric gap

indicates the Fano resonance described by a quantum interference between tunneling paths into the Kondo resonance and into the conduction-band states[23]. The dI/dV spectrum with such a quantum interference can be expressed by the Fano equation[24] as

$$\frac{dI}{dV} \propto A \cdot \frac{(q+\varepsilon)^2}{(1+\varepsilon)^2} + B, \quad \varepsilon = \frac{eV - E_0}{\Gamma} \tag{1}$$

where Γ is a half width at half maximum of the size of the hybridization gap, E_0 is the peak (dip) position of the Kondo resonance with respect to the Fermi energy, and q, so-called a q factor, describes the lineshape of the Fano resonance, respectively. The relationship between Γ and the Kondo temperature T_k can be expressed as $2\Gamma = \sqrt{(5.4k_BT)^2 + (2k_BT_K)^2}$ for finite temperatures T[25]. In this study, the experimental dI/dV spectrum is simulated with a standard Fano model to extract Γ and T_k, while the importance of advanced analyses such as a cotunnleing model or the Fano model with the Gaussian peak fitting is proposed to fully describe the dI/dV spectra especially at higher energy ranges in the Kondo lattice system[9,12]. The evaluated Γ of ~ 21.6 meV from the Fano fit to the dI/dV spectrum recorded at 80 K gives T_k of ~ 150 K [see the dotted line in Fig. 5(b)], in good agreement with the recent ARPES studies[7]. A drastic change occurs in the dI/dV spectrum with decreasing temperature. We find the emergence of the in-gap state with a characteristic peak-dip feature inside the Kondo hybridization gap at 4.4 K. The observed temperature dependence of the dI/dV spectrum is also reported by previous STM studies on the cleaved SmB_6(001) surfaces[9,12], thus ensuring intrinsic electronic properties of the SmB_6(001) surface prepared by Ar^+ ion sputtering and annealing in this study.

A remaining question is whether the observed in-gap state dominantly reflect surface- or bulk- related characters. We here discuss the robustness of the in-gap state with a pronounced peak structure located at ~ −8 meV against spatial variations. Since surface states are expected to be more sensitive to the surface disorder often induced by defects than bulk states, the comparison of the dI/dV spectra recorded on ordered and disordered regions would provide the additional information on the nature of the in-gap state. Figure 5(c) displays the spatial dependence of the dI/dV spectra near the Fermi energy recorded on ordered and disordered regions of the SmB_6(001) surface at 4.4 K. The pronounced peak structure observed on the ordered region is noticeably suppressed on the disordered region near defects.

According to the atomic-scale spatial dependence measurements of the dI/dV spectra (Supplementary Fig. S1), the peak intensity is significantly reduced near defects. However, even atop the defect, the peak structure still remains and the intensity is minimum. The peak intensity significantly recovers at the ordered site even 0.5 nm apart from the defect as shown in Fig. S1(c). On the ordered region, the peak intensity exhibits no essential site dependence. These results reveal that the in-gap state with the pronounced peak structure is sensitive to the structural variation on the surface, but survives on the whole surface irrespective of defects. The observed structural robustness of the in-gap state would be related to the topological protection that is one of the main characteristics as a topological surface state. Note that, as a consequence of the reduction of the peak intensity located at −8 meV near the defect, the fine shoulder structure indicated by the arrow in Fig. 5(b) is clearly recognized as a peak structure at −15 meV [See the dotted line in Supplementary Fig. S1(d)]. Its energy position and intensity are almost independent of the structural variation on the surface. Thus, in contrast to the surface-state-derived peak structure located at −8 meV, the localized bulk f-states could dominantly contribute to this peak structure as recently reported for the cleaved SmB_6(001) surface by STM measurements at lower temperatures with a lower bias-voltage modulation[12].

In summary, real-space surface characterizations by STM successfully prove the formation of the Sm-terminated single-phase SmB_6(001) surface with a non-reconstructed $p(1 \times 1)$ lattice by Ar^+ ion sputtering and controlled annealing. Temperature and spatial dependent spectroscopic measurements near the Fermi energy indicated that the in-gap state emerging inside the Kondo hybridization gap at 4.4 K is a robust surface state against structural variations, which could reflect the intrinsic electronic properties of SmB_6 potentially as a topological Kondo insulator. The validity of Ar^+ ion sputtering and controlled annealing to reproducibly achieve the single-phase SmB_6(001) surface demonstrated here allows the access for intrinsic electronic properties of SmB_6 by spatially-integrated techniques towards application purposes as well as further fundamental researches in material science.

Methods

SmB_6(001) single crystal. In this study, the same SmB_6(001) single crystal as in ref.[13] was used, which had been grown by the floating-zone melting method[26], then cut and polished along the (001) plane determined by Laue x-ray diffraction. The surface was prepared *in situ* by repeated cycles of Ar^+ ion sputtering with 1.0 keV energy and subsequent controlled annealing. The annealing temperature was measured on the SmB_6(001) crystal using a pyrometer.

Measurement conditions. STM measurements were performed in ultrahigh vacuum ($< 4.0 \times 10^{-11}$ mbar) at 4.4 and 80 K by using electrochemically-etched W tips. The differential conductance spectra, dI/dV, were recorded using a lock-in technique with a bias-voltage modulation of 3 and 20 mV at 722 Hz. Spatially-averaged structural information of the surface was also investigated by LEED at room temperature.

References

1. Coleman, P. *Heavy Fermions: Electrons at the Edge of Magnetism, Handbook of Magnetism and Advanced Magnetic Materials*, Vol 1, 95-148 (Wiley 2007).
2. Menth, A., Buehler, E. & Geballe, T. H. Magnetic and Semiconducting Properties of SmB_6. *Phys. Rev. Lett.* **22**, 295 (1969).
3. Nanba, T. *et al.* Gap state of SmB_6. *Physica B* **186–188**, 440–443 (1993).
4. Dzero, M., Sun, K., Galitski, V. & Coleman Topological Kondo Insulators. *P. Phys. Rev. Lett.* **104**, 106408 (2010).

5. Lu, F., Zhao, J., Weng, H., Fang, Z. & Dai, X. Correlated topological insulators with mixed valence. *Phys. Rev. Lett.* **110**, 096401 (2013).
6. Neupane, M. *et al.* Surface electronic structure of the topological Kondo-insulator candidate correlated electron system SmB_6. *Nat. Commun.* **4**, 2991 (2013).
7. Jiang, J. *et al.* Observation of possible topological in-gap surface states in the Kondo insulator SmB_6 by photoemission. *Nat. Commun.* **4**, 3010 (2013).
8. Yee, M. M. *et al.* Imaging the Kondo Insulating Gap on SmB_6. arXiv:1308.108.
9. Ruan, W. *et al.* Emergence of a Coherent In-Gap State in the SmB_6 Kondo Insulator Revealed by Scanning Tunneling Spectroscopy. *Phys. Rev. Lett.* **112**, 136401 (2014).
10. Rößler, S. *et al.* Hybridization gap and Fano resonance in SmB_6. *Proc. Natl. Acad. Sci. USA* **111**, 4798–4802 (2014).
11. Rößler, S. *et al.* Surface and electronic structure of SmB_6 through scanning tunneling microscopy. *Philos. Mag.* **96**, 3262–3273 (2016).
12. Jiao, L. *et al.* Additional energy scale in SmB_6 at low-temperature. *Nat. Commun.* **7**, 13762 (2016).
13. Ellguth, M., Tusche, C., Iga, F. & Suga, S. Momentum microscopy of single crystals with detailed surface characterisation. *Philos. Mag.* **96**, 3284–3306 (2016).
14. Ramankutty, S. V. *et al.* Comparative study of rare earth hexaborides using high resolution angle-resolved photoemission. *J. Electron Spectrosc. Relat. Phenom.* **208**, 43–50 (2016).
15. Aono, M., Nishitani, R., Tanaka, T., Bannai, E. & Kawai, S. Azimuthal anisotropy in low-energy ion scattering from SmB_6(001). *Solid State Commun.* **28**, 409–412 (1978).
16. Miyazaki, H., Hajiri, T., Ito, T., Kunii, S. & Kimura, S. Momentum-dependent hybridization gap and dispersive in-gap state of the Kondo semiconductor SmB_6. *Phys. Rev. B* **86**, 075105 (2012).
17. Swanson, L. & McNeely, D. Work functions of the (001) face of the hexaborides of Ba, La, Ce and Sm. *Surf. Sci.* **83**, 11–28 (1979).
18. Miyamachi, T. *et al.* Epitaxially stabilized iron thin films via effective strain relief from steps. *Phys. Rev. B* **94**, 045439 (2016).
19. Ishizaka, A. & Doi, T. Systematic change in surface structures on Si(111) clean surfaces with temperature. *Philos. Mag. Lett.* **65**, 95 (1992).
20. Homma, Y., Hibino, H., Ogino, T. & Aizawa, N. Sublimation of the Si(111) surface in ultrahigh vacuum. *Phys. Rev. B* **55**, 10237 (1997).
21. Lange, G., Meli, C. A., Toennies, J. P. & Greene, E. F. Helium atom scattering from the Si(111) surface at high temperatures. *Phys. Rev. B* **56**, 4642 (1997).
22. Zhu, Z. H. *et al.* Polarity-Driven Surface Metallicity in SmB_6. *Phys. Rev. Lett.* **111**, 216402 (2013).
23. Madhavan, V., Chen, W., Jamneala, T., Crommie, M. F. & Wingreen, N. Tunneling into a Single Magnetic Atom: Spectroscopic Evidence of the Kondo Resonance. *Science* **280**, 567–569 (1998).
24. Fano, U. Effects of configuration interaction on intensities and phase shifts. *Phys. Rev.* **124**, 1866 (1961).
25. Nagaoka, K., Jamneala, T., Grobis, M. & Crommie, M. F. Temperature dependence of a single Kondo impurity. *Phys. Rev. Lett.* **88**, 077205 (2002).
26. Keck, P. H., Green, M. & Polk, M. L. Shapes of Floating Liquid Zones between Solid Rods. *J. Appl. Phys.* **24**, 1479–1481 (1953).

Acknowledgements

This work is partly supported by JSPS KAKENHI for Young Scientists (A), Grant No. 16H05963, for Scientific Research (B), Grant No. 26287061, Hoso Bunka Foundation, Shimadzu Science Foundation, Iketani Science and Technology Foundation.

Author Contributions

T.M., S.S., and F.K. conceived and designed the experiments. F.I. grew the SmB_6 single crystal. S.S., M.E., C.T., and C.M.S. carried out initial surface characterization experiments. T.M., S.S., and F.K. carried out STM and LEED experiments. T.M. analyzed the data. T.M., S.S., and F.K. wrote the paper with inputs from all authors. All authors discussed the results and commented on the manuscript.

Additional Information

Supplementary information accompanies this paper at https://doi.org/10.1038/s41598-017-12887-2.

Competing Interests: The authors declare that they have no competing interests.

Publisher's note: Springer Nature remains neutral with regard to jurisdictional claims in published maps and institutional affiliations.